NASA TECHNICAL NOTE

NASA TN D-4733

EFFECT OF CHAMBER PRESSURE, FLOW PER ELEMENT, AND CONTRACTION RATIO ON ACOUSTIC-MODE INSTABILITY IN HYDROGEN-OXYGEN ROCKETS

by John P. Wanhainen, Charles E. Feiler, and C. Joe Morgan

Lewis Research Center
Cleveland, Ohio

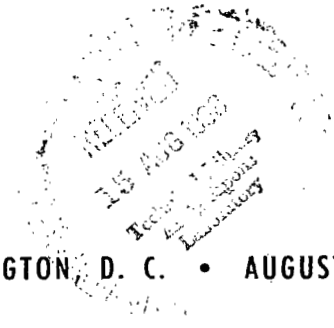

NATIONAL AERONAUTICS AND SPACE ADMINISTRATION • WASHINGTON, D. C. • AUGUST 1968

NASA TN D-4733

EFFECT OF CHAMBER PRESSURE, FLOW PER ELEMENT, AND CONTRACTION RATIO ON ACOUSTIC-MODE INSTABILITY IN HYDROGEN-OXYGEN ROCKETS

By John P. Wanhainen, Charles E. Feiler, and C. Joe Morgan

Lewis Research Center
Cleveland, Ohio

NATIONAL AERONAUTICS AND SPACE ADMINISTRATION

For sale by the Clearinghouse for Federal Scientific and Technical Information
Springfield, Virginia 22151 – CFSTI price $3.00

ABSTRACT

An experimental investigation of a 20 000-lb- (89-kN-) thrust engine with a single coaxial-type injector was conducted to determine the effect of variations in chamber pressure, weight flow per element, and contraction ratio, by changing nozzle throat diameter, on tangential-acoustic-mode stability characteristics of hydrogen-oxygen rocket engines. These characteristics were evaluated by determining the hydrogen-injection temperature below which combustion was unstable. A correlation of the stability limits was obtained as a function of the variables investigated. The roles of various parameters were also interpreted according to the mechanism assumed in the response-factor model of this propellant combination.

EFFECT OF CHAMBER PRESSURE, FLOW PER ELEMENT, AND CONTRACTION RATIO ON ACOUSTIC-MODE INSTABILITY IN HYDROGEN-OXYGEN ROCKETS

by John P. Wanhainen, Charles E. Feiler, and C. Joe Morgan

Lewis Research Center

SUMMARY

An experimental investigation was conducted at the NASA Lewis Research Center to determine the effect of variations in the following parameters on the tangential-acoustic-mode stability characteristics of hydrogen-oxygen rocket engines: (1) chamber pressure from 125 to 475 psia (862 to 3275 kN/m^2 abs), (2) weight flow per element from 0.064 to 0.192 pound mass per second (0.0291 to 0.0872 kg/sec), and (3) contraction ratio from 1.5 to 4.5 with changes in nozzle throat diameter.

The experiments were performed with a 20 000-pound- (88.96-kN-) thrust engine with a single coaxial-type injector. The stability characteristics were evaluated by determining the hydrogen-injection temperature below which combustion was unstable.

Changes in chamber pressure effected by throttling the total weight flow had no effect on the hydrogen-temperature stable operating limits. Decreasing the contraction ratio at either constant weight flow or constant chamber pressure lowered the hydrogen-temperature stable operating limits. A correlation of the stability limits was obtained as a function of the several variables studied, so that the parameter

$$\left(\frac{2g\,\Delta P_H}{\rho_H}\right)^{1/2} \rho_O (D_O)^{1.25} \left(\frac{1}{O/F}\right)^{1/2}$$

where ΔP_H is the hydrogen-injector pressure drop, ρ_H is the hydrogen-injection density, ρ_O is the oxygen-injection density, D_O is the oxygen-injection orifice diameter, and O/F is the oxidant-fuel ratio, has a constant value at the limit separating stable and unstable operation. The roles of the various parameters were also interpreted according to the mechanism assumed in the response-factor model of this hydrogen-oxygen propellant combination.

INTRODUCTION

In the selection of operating parameters and thrust-chamber geometry for a new rocket propulsion system, the designer must give consideration to several factors, such as thrust-chamber cooling, system weight, engine envelope, combustion performance, and combustion stability. With the exception of combustion stability, the factors are, in general, amenable to analyses. However, much less is known about the effect of engine operating parameters and chamber geometry on combustion stability. Accordingly, the primary objective of the investigation reported herein was to assess the effect of several design variables of chamber pressure, weight flow per element (thrust per element), and contraction ratio on combustion stability. The effect of oxygen-injection temperature (or density) was also studied in a limited number of tests. Emphasis was placed on the tangential-mode acoustic instability, which is frequently encountered and difficult to eliminate in rocket-engine development programs.

The present experimental stability-limit data and those of reference 1 were analyzed with the objective of obtaining a correlation that would predict the effect of the different variables and provide some insight into the mechanism that influences the stability of hydrogen-oxygen engines. The present experimental stability data are also compared with the stability limits calculated by the analysis of reference 2, hereinafter referred to as the response-factor model. In this model, the role of hydrogen in instability was assumed to be determined by the dynamic response of the hydrogen flow to chamber pressure perturbations. Reference 2 showed that, at low values of hydrogen-injection pressure drop (low hydrogen temperature), the hydrogen flow could couple in phase with the chamber pressure perturbation at an amplitude sufficient to drive instability. The variations in stability limits with operating conditions and thrust-chamber geometry are considered herein with respect to this coupling mechanism.

The investigation, conducted in the Rocket Engine Test Facility, used a hydrogen-oxygen rocket that was 10.78 inches (27.36 cm) in diameter. The standard engine, which had a contraction ratio of 1.9, produced a sea-level thrust of about 20 000 pounds (88.96 kN) at a chamber pressure of 300 psia (2070 kN/m^2 abs). The experimental program included variations in (1) chamber pressure from 125 to 475 psia (862 to 3275 kN/m^2 abs), (2) weight flow per element from 0.064 to 0.192 pound mass per second (0.0291 to 0.0872 kg/sec), and (3) contraction ratio from 1.5 to 4.5 (nominal) with changes made in the exhaust nozzle throat diameter. In addition to the previously mentioned stability data, the performance of the engine at the various conditions is also presented.

SYMBOLS

A	area, $in.^2$; cm^2
α	contraction ratio
D	injector orifice diameter, in.; cm
E	number of injection elements
g	gravitational conversion factor, (lb mass/lb force)(in. $/sec^2$); (kg/kN)(m/sec^2)
N_{H_2}	hydrogen response factor
O/F	oxidant-fuel ratio
P	pressure, psia; kN/m^2 abs
ΔP	injector pressure drop, psi; kN/m^2
T	temperature, ^oR; K
W	propellant flow rate, lb/sec; kg/sec
ψ_{cr}	stability parameter, lb mass/($in.^{3/4}$ sec); kg/($m^{3/4}$ sec)
η_{C*}	characteristic-exhaust-velocity efficiency, percent
ρ	density, lb mass/$in.^3$; kg/m^3
σ	standard deviation

Subscripts:

c	chamber
H	hydrogen
O	oxygen
t	total
th	nozzle throat
tr	transition quantity

APPARATUS

Test Facility

The Rocket Engine Test Facility of the Lewis Research Center is a remotely operated

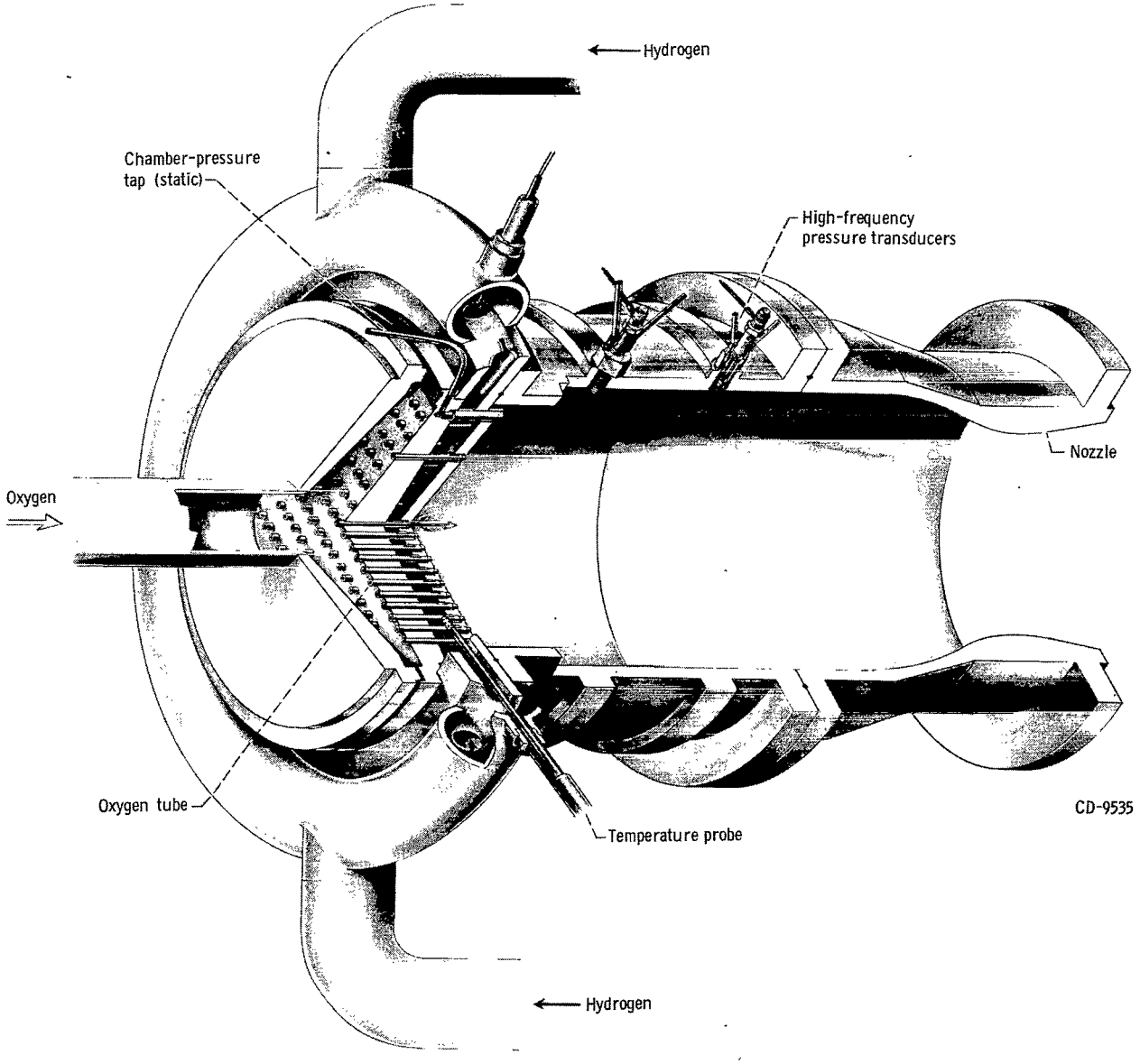

Figure 1. - Rocket engine.

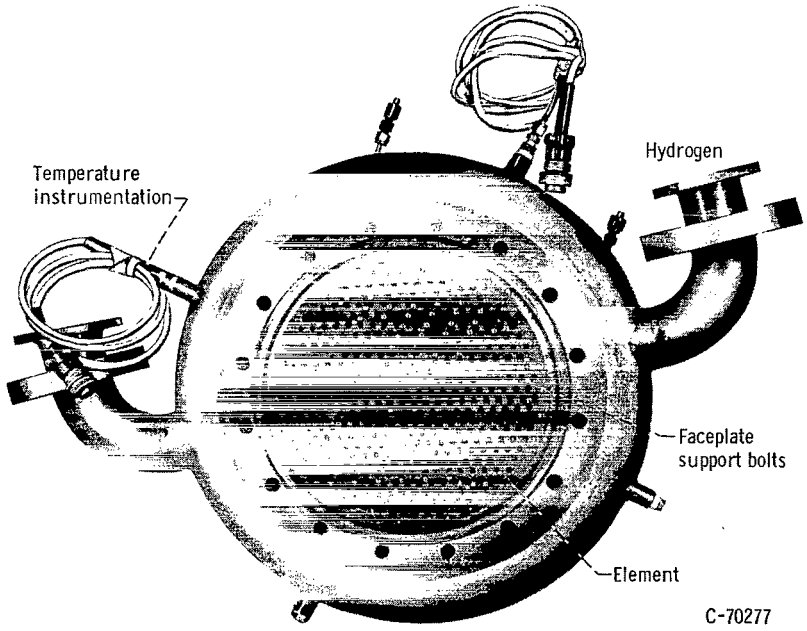

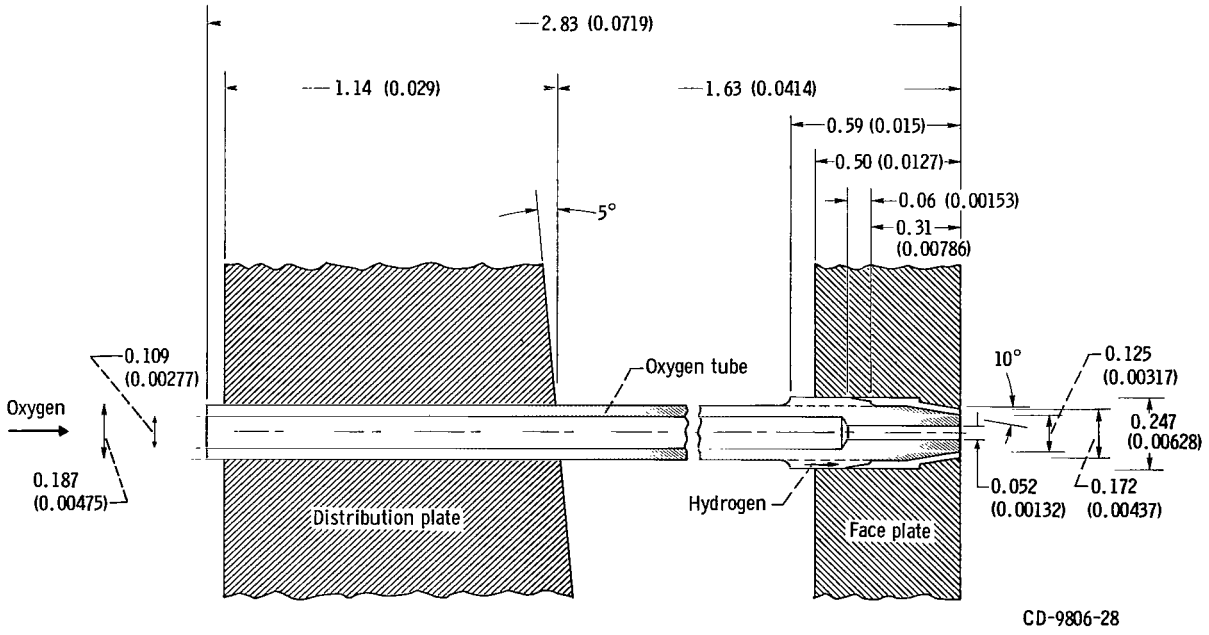

Figure 2. - Faceplate and cross-sectional views of 421-element, removable copper face, 10.78-inch (0.274-m-) diameter concentric-tube injector. (All dimensions are in inches (meters) unless noted otherwise.)

50 000-pound- (222. 5-kN-) thrust sea-level stand. The facility utilized a pressurized propellant system to deliver the propellants to the engine from the storage tanks. The oxygen propellant line was immersed in a nitrogen bath, and the liquid-hydrogen line was insulated with a plastic-type foam. The propellant storage tanks consisted of 75- and 175-cubic-foot (2. 12- and 4. 95-cu m) liquid-hydrogen Dewars, a 120 000-standard-cubic-foot (3400-cu m), gaseous-hydrogen bottle farm, and a 55-cubic-foot (1. 56-cu m) liquid-oxygen tank submerged in a liquid-nitrogen bath. Sketches and a more detailed description of the facility are given in reference 1.

Engine

The rocket engine (fig. 1) comprised an injector with a removable faceplate, a cylindrical heat-sink thrust chamber with a 10. 78-inch (27. 36-cm) inside diameter, and a convergent-divergent heat-sink exhaust nozzle. The length of the cylindrical section of the combustor was about 12. 75 inches (32. 38 cm). The nozzle convergence half-angle was 30°, and the contraction ratio was varied by changing the throat diameter and the length of the subsonic portion of the nozzle. The inner surfaces of the mild-steel thrust chamber and nozzle were coated with 0. 030-inch- (0. 076-cm-) thick flame-sprayed zirconium oxide. This coating allowed a run duration of about 3 seconds, which was adequate to obtain the required data.

Faceplate and cross-sectional views of the 421-element concentric-tube injector are presented in figure 2. The faceplate was fabricated from 0. 50-inch- (1. 27-cm-) thick oxygen-free copper, a material with a good heat-sink capability; thus, the need for careful attention to coolant-flow requirements within the injector was eliminated. The hydrogen-injection area was 4. 62 square inches (29. 8 sq cm), and the oxygen-injection area was 0. 89 square inch (5. 74 sq cm).

Hydrogen Temperature Controller

The hydrogen-temperature ramp was accomplished by the following procedure: The run was started with a mixture of liquid hydrogen and warm gaseous hydrogen. Then the percentage of gas was reduced in a predetermined ramp while the liquid-hydrogen valve was simultaneously opened to maintain a constant total flow. The liquid was swirled into the gaseous-hydrogen stream to accomplish mixing. The mixing station was outside the injector in a manifold with an intervening volume of 1140 cubic inches (0. 0187 cu m). A schematic diagram of the mixer is shown in figure 3. Flow rates of gaseous hydrogen

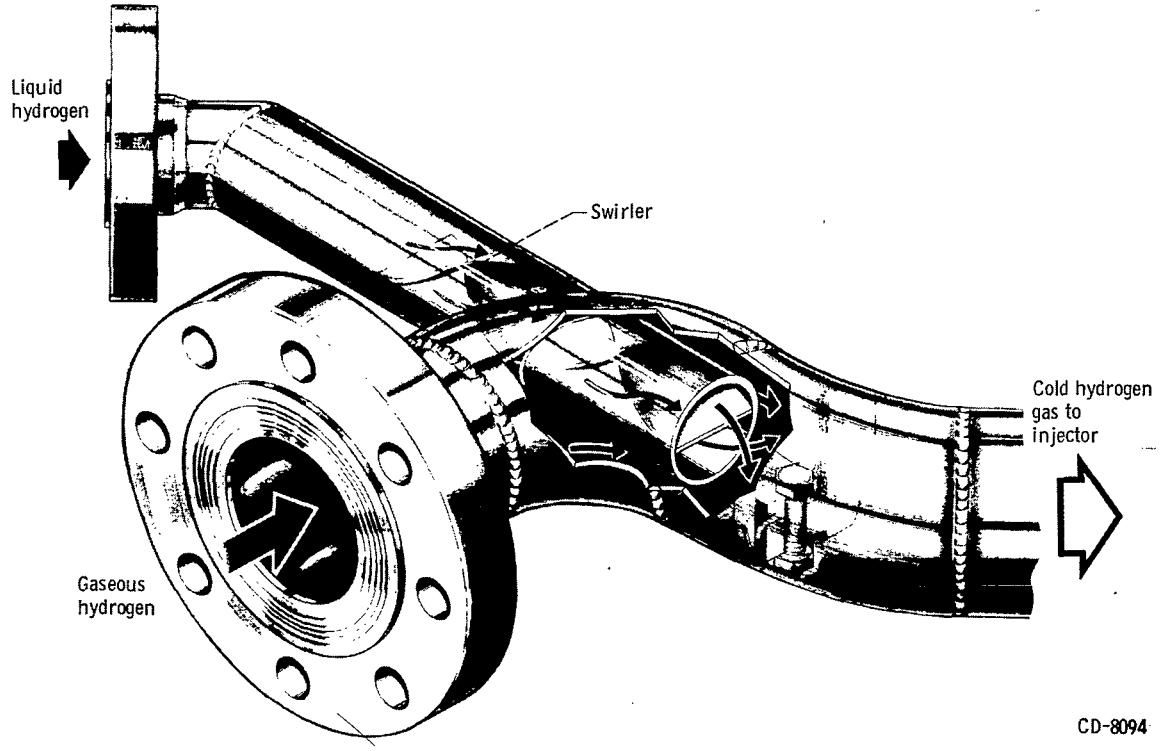

Figure 3. - Schematic diagram of mixing station.

and liquid hydrogen to the mixer were controlled with valves that were operated by an electrohydraulic servosystem.

Instrumentation

The instrumentation used in the investigation and the locations for the various transducers are shown in the diagram of the engine and associated plumbing in figure 4. The signals from the transducers were transmitted to the automatic digital data recording system at Lewis. Piezoelectric-type, water-cooled, flush-mounted pressure transducers were used at three locations on the thrust chamber to determine the character and phase relation of the pressure field and to allow identification of the screech mode. The response characteristics of the transducers were flat to within 10 percent to a frequency of 10 000 cps (10 000 Hz) and had a nominal resonant frequency of 20 000 cps (20 000 Hz) in the water-cooled mount. The signals from high-frequency-response transducers were recorded on magnetic tape and, in addition, were displayed on direct-reading instruments for visual monitoring during the tests.

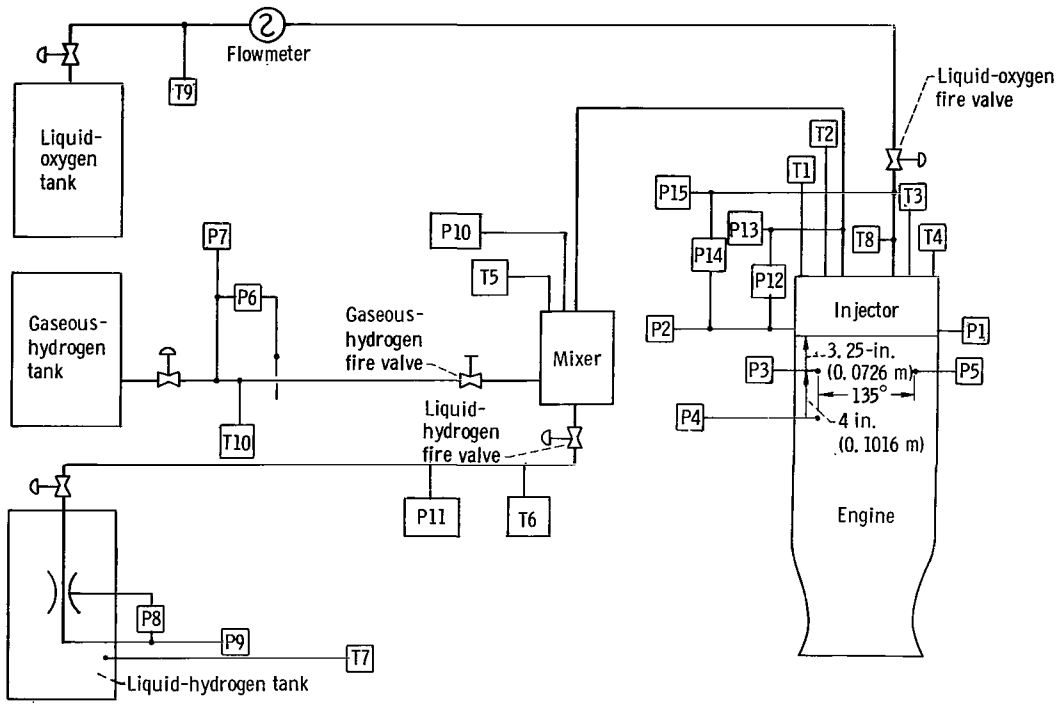

P1 Static chamber pressure (injector face), four-arm strain-gage transducer 1
P2 Static chamber pressure (injector face), four-arm strain-gage transducer 2
P3 Dynamic chamber pressure, water-cooled quartz pressure transducer 3
P4 Dynamic chamber pressure, water-cooled quartz pressure transducer 4
P5 Dynamic chamber pressure, water-cooled quartz pressure transducer 5
P6 Gaseous-hydrogen orifice differential pressure, four-arm strain-gage transducer
P7 Gaseous-hydrogen orifice pressure, four-arm strain-gage transducer
P8 Liquid-hydrogen venturi differential pressure, four-arm strain-gage type
P9 Liquid-hydrogen venturi pressure, four-arm strain-gage transducer
P10 Hydrogen-mixer pressure, four-arm strain-gage transducer
P11 Liquid-hydrogen line pressure, four-arm strain gage transducer
P12 Hydrogen-injection differential pressure, four-arm strain-gage transducer
P13 Hydrogen-injection pressure, four-arm strain-gage transducer
P14 Oxygen-injection differential pressure, four-arm strain-gage transducer
P15 Oxygen-injection pressure, four-arm strain-gage transducer
T1 Hydrogen-injector temperature, carbon resistor sensor probe 1
T2 Hydrogen-injector temperature, carbon resistor sensor probe 2
T3 Hydrogen-injector temperature, carbon resistor sensor probe 3
T4 Hydrogen-injector temperature, carbon resistor sensor probe 4
T5 Hydrogen-mixer temperature, carbon resistor sensor probe
T6 Liquid-hydrogen line temperature, carbon resistor sensor probe
T7 Liquid-hydrogen venturi temperature, platinum type
T8 Oxygen-injection temperature, copper-constantan thermocouple
T9 Oxygen flowmeter temperature, platinum type
T10 Gaseous-hydrogen orifice temperature, iron-constantan thermocouple

Figure 4. - Test instrumentation and transducer locations.

Oxygen propellant weight flow was determined with a vane-type flowmeter that was water calibrated with a static weighing system. The correction from water calibration to cryogenic calibration was obtained from the flowmeter manufacturer. Liquid-hydrogen weight flow was measured by using a venturi, and the gaseous-hydrogen weight flow was measured using an orifice plate. The strain-gage-type pressure transducers were calibrated by a commercial standard. Liquid flow temperatures were measured by platinum-resistance-type sensors described in reference 3. The hydrogen-injection temperature was measured using four carbon-resistance-type probes (ref. 4), installed as illustrated in figure 1. Immediately prior to the data acquisition, the pressure system was calibrated by an electrical two-step calibration system, which used resistances in an electrical circuit to simulate a given pressure.

PROCEDURE

The experimental evaluation of the effects of changing chamber pressure, weight flow per element, and contraction ratio is complicated by the common difficulty of not being able to vary one parameter at a time while maintaining the other two constant. To circumvent this problem, three series of tests were conducted wherein different pairs of parameters were varied so that the effect of each parameter alone could be determined from the complete matrix. The matrix is shown in table I, which indicates the parameters that were varied and the one that was held constant for each series.

TABLE I. - NOMINAL TEST CONDITIONS

Test series	Chamber pressure, P_c		Weight flow per element, W_t/E		Thrust per element		Contraction ratio, ε	Nozzle throat diameter	
	psia	kN/m^2 abs	lb/sec	kg/sec	lb	N		in.	cm
A	125	862	0.064	0.0291	20	89	1.9	7.82	19.85
	190	1310	.096	.0436	30	133	↓	↓	↓
	300	2070	.152	.069	48	214			
	380	2620	.192	.0872	60	267			
B	300	2070	0.064	0.0291	20	89	4.5	5.04	12.8
	↓	↓	.096	.0436	30	133	3.0	6.22	15.8
			.152	.069	48	214	1.9	7.82	19.85
			.192	.0872	60	267	1.5	8.78	22.3
C	475	3275	0.152	0.069	48	214	3.0	6.22	15.8
	300	2070	.152	.069	48	214	1.9	7.82	19.85
	235	1620	.152	.069	48	214	1.5	8.78	22.3

The effects of changes in the engine operating parameters and the thrust-chamber geometry were evaluated by ramping the hydrogen-injection temperature down into screech and determining the change in hydrogen-temperature stable operating limits. A typical oscillograph record of a test to determine the stable operating limits of a combustor in terms of hydrogen-injection temperature is presented in figure 5. An initial hydrogen temperature was selected by presetting the valves of the mixer and, about 1 second after ignition, ramping the gas valve toward a closed position while simultaneously opening the liquid valve to reduce the temperature of the injected hydrogen to a value below the anticipated screech limit. The operating conditions at the onset of instability were then obtained from high-speed recorder data. The time of transition into screech was indicated by an oscillograph trace of a flush-mounted pressure transducer. Combustion was considered unstable when a periodic waveform with an amplitude greater than the noise level (10 to 15 psi or 69 to 103 kN/m^2 peak to peak) was observed on the

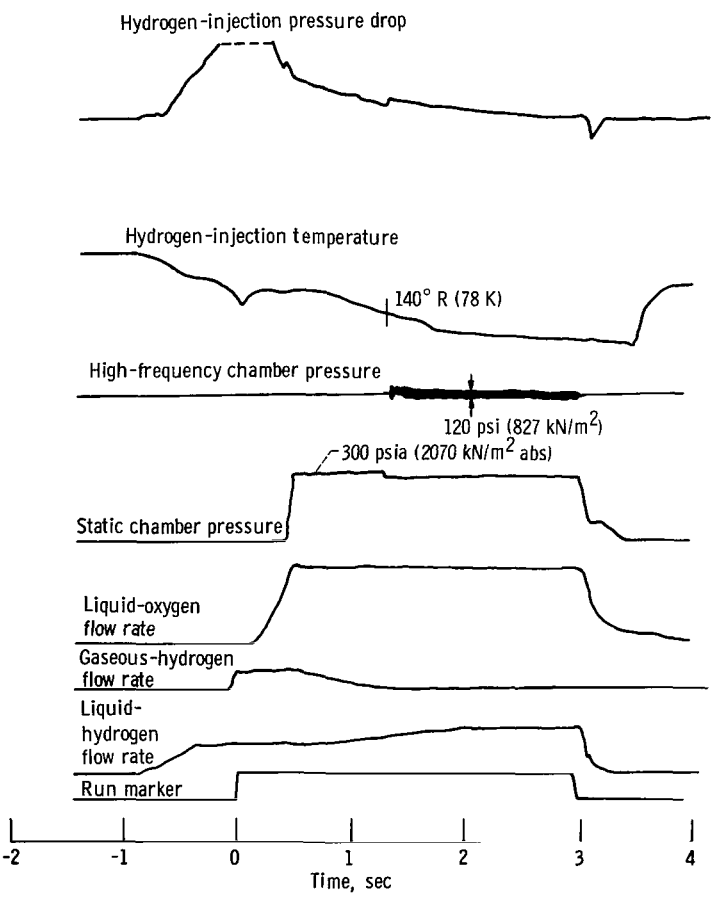

Figure 5. - Oscillograph traces of typical screech test illustrating hydrogen-temperature-rating technique.

oscillograph record. Tests were repeated at different oxidant-fuel ratios to obtain stability-limit curves.

RESULTS AND DISCUSSION

The results and accompanying discussions are presented in six sections: (1) stability characteristics, (2) screech characteristics, (3) combustion performance, (4) correlation of stability data, (5) application of the response-factor model to experiment, and (6) application and interpretation of results. The experimental data are presented in table II.

Stability Characteristics

Effect of chamber pressure and weight flow per element at constant contraction ratio. - Test series A consisted of four groups of runs made by throttling the total weight flow to vary the chamber pressure from 125 to 380 psia (862 to 2620 kN/m^2 abs). The contraction ratio (nozzle throat diameter) was held constant at 1.9. Typical results are shown in figure 6 where the hydrogen-injection temperature at the instant of screech

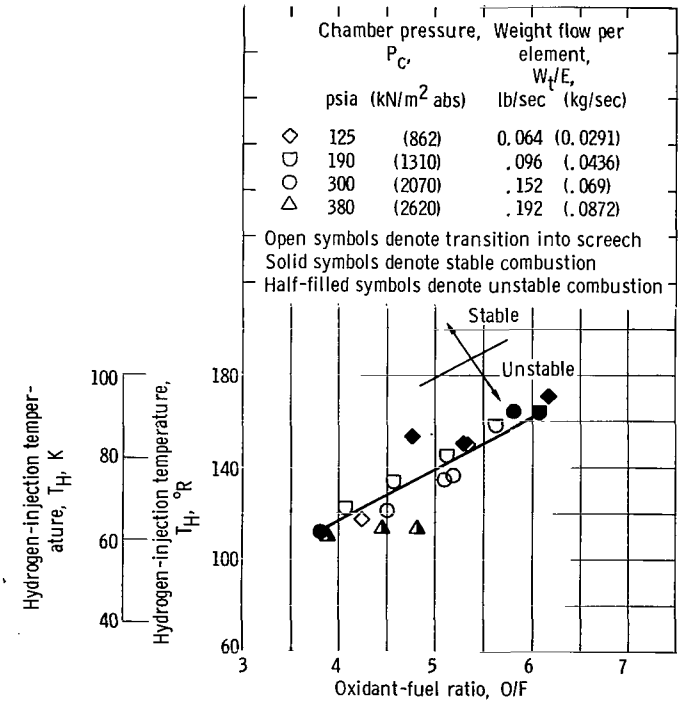

Figure 6. - Effect of chamber pressure on variation of screech transition temperature. Contraction ratio, 1.9

TABLE II. - EXPERIMENTAL DATA

(a) U.S. customary units

Test series	Test	Contraction ratio, $\mathscr{A}$	Hydrogen injection-temperature, T_H, ^oR	Static pressure at injector, P, psia	Injector pressure drop, psi		Propellant weight flow, lb/sec		Oxidant-fuel ratio, O/F	Efficiency of characteristic exhaust velocity, η_{C^*}, percent	Stability-limit parameter, $\mathscr{W}_{cr}$, $(2g\,\Delta P_H/\rho_H)^{1/2}\rho_O(D_O)^{1.25}(1/(O/F))^{1/2}$, (lb mass/sec)(1/in.$^{3/4}$)	Stability classification
					Hydrogen, ΔP_H	Oxygen, ΔP_O	Hydrogen, W_H	Oxygen, W_O				
C	38	1.5	121	239	24.7	129.0	9.29	45.71	4.92	100.8	4.386	Transition
	39	↓	101	240	32.5	127.5	11.00	43.57	3.96	99.2	4.922	↓
	40		147	245	26.5	152.0	8.47	49.62	5.86	101.0	4.577	
	41		104	245	26.0	123.4	10.26	45.37	4.42	100.4	4.208	
	42		133	247	28.0	133.0	9.10	48.25	5.30	104.1	4.678	Stable
	44		132	245	26.4	145.0	9.06	48.54	5.36	100.4	4.482	Transition
A	57	1.9	145	198	19.5	73.2	6.31	32.85	5.13	99.1	4.674	Transition
	58		122	199	23.2	65.2	7.37	30.03	4.07	99.7	5.119	Transition
	59		164	202	15.5	70.5	5.61	34.05	6.07	101.8	4.165	Stable
	60		134	200	21.2	81.4	6.99	32.15	4.59	97.1	4.796	Transition
	61		159	201	20.0	77.8	5.96	33.64	5.64	99.9	4.655	Transition
	62		149	136	15.4	30.4	4.20	21.99	5.24	101.0	5.187	Stable
	63		151	135	14.0	38.7	4.19	22.17	5.28	99.8	4.811	Transition
	64		117	135	14.2	32.9	4.79	20.34	4.25	101.1	4.701	Transition
	65		171	136	16.7	35.0	3.70	23.53	6.19	103.1	5.357	Stable
	66		153	136	14.7	28.7	4.45	21.22	4.77	101.6	5.383	Stable
	67		113	396	----	261.0	13.40	64.83	4.84	96.7	-----	Unstable
	68		111	399	----	235.0	15.68	60.79	3.88	97.6	-----	Unstable
	70	↓	113	397	----	254.0	14.21	63.36	4.46	96.9	-----	Unstable
B	255	3.0	261	270	12.5	68.9	5.84	31.27	5.35	93.2	4.324	Transition
	256	↓	146	289	18.0	61.8	7.26	28.36	3.90	100	4.269	↓
	257		244	288	13.0	75.3	5.79	33.45	5.78	95.4	3.966	
	258		149	310	18.5	73.4	7.13	31.22	4.39	100.2	4.003	
	259		167	301	19.0	67.2	6.72	31.32	4.66	99.0	4.272	
	290		233	271	14.2	71.2	5.31	32.57	6.13	-----	4.045	
	291		130	275	21.0	56.4	7.99	29.38	3.67	-----	4.536	↓
	292		124	320	34.9	61.5	8.37	29.22	3.49	101.5	5.417	Stable
	293		164	307	20.0	71.8	6.66	31.55	4.74	98.2	4.224	Transition
	294	↓	199	316	17.2	88.0	6.52	34.51	5.29	95.8	4.066	Transition

TABLE II. - Continued. EXPERIMENTAL DATA

(a) Continued. U.S. customary units

Test series	Test	Contraction ratio, $\mathscr{A}$	Hydrogen injection-temperature, T_H, ^oR	Static pressure at injector, P, psia	Injector pressure drop, psi		Propellant weight flow, lb/sec		Oxidant-fuel ratio, O/F	Efficiency of characteristic exhaust velocity, η_{C^*}, percent	Stability-limit parameter, $\mathscr{W}_{cr}$, $(2g\Delta P_H/\rho_H)^{1/2}\rho_O(D_O)^{1.25}(1/(O/F))^{1/2}$, (lb mass/sec)(1/in.$^{3/4}$)	Stability classification
					Hydrogen, ΔP_H	Oxygen, ΔP_O	Hydrogen, W_H	Oxygen, W_O				
B	274	4.5	351	316	14.7	42.3	4.01	24.10	6.00	96.9	4.640	Stable
	275		270	317	11.0	47.3	4.37	25.20	5.76	91.7	3.697	Transition
	277		230	315	13.0	44.7	4.79	23.40	4.89	93.2	4.036	
	279		174	315	15.0	39.9	5.27	21.30	4.03	96.9	4.122	
	280		191	316	13.8	41.9	5.22	22.90	4.40	92.2	3.982	
	281		354	316	17.5	59.4	4.32	28.10	6.49	----	5.048	
	282		242	316	18.8	57.4	5.30	27.30	5.16	----	4.838	
	326	1.5	115	346	40.0	246.4	13.79	66.20	4.80	98.7	4.423	Transition
	327		126	354	40.0	280.8	12.45	69.98	5.62	100.6	4.323	
	328		109	327	46.5	100.9	13.74	60.30	4.39	99.7	4.916	
	329		122	351	35.5	277.9	12.87	68.91	5.35	99.6	4.094	
	330		121	348	45.5	297.0	12.92	70.66	5.47	97.1	4.493	
A, B, and C	331	1.9	112	332	39.5	139.5	12.69	48.36	3.81	100.3	4.951	Transition
	333		135	358	39.5	181.5	11.06	56.51	5.11	100.9	4.701	Transition
	335		164	339	57.5	175.5	9.61	55.86	5.81	101.0	6.116	Stable
	336		120	329	33.5	144.3	11.20	50.30	4.51	100.1	4.453	Transition
	337		136	340	32.5	162.3	10.41	53.98	5.18	100.8	4.412	Transition
C	493	3.0	135	501	23.7	153.2	12.85	46.98	3.66	101.8	3.701	Transition
	494		243	472	25.4	185.3	9.19	52.33	5.69	98.4	4.591	
	495		156	496	20.1	157.3	11.42	50.56	4.43	97.8	3.641	
	496		253	471	28.7	178.8	9.50	51.89	5.46	97.7	5.087	

TABLE II. - Continued. EXPERIMENTAL DATA

(a) Concluded. U.S. customary units

Test series	Test	Contraction ratio, $\mathscr{A}$	Injection temperature, ^{o}R		Static pressure at injector, P, psia	Injector pressure drop, psi		Propellant weight flow, lb/sec		Oxidant-fuel ratio, O/F	Efficiency of characteristic exhaust velocity, η_{C^*}, percent	Stability-limit parameter, $\mathscr{W}_{cr}$, $(2g\,\Delta P_H/\rho_H)^{1/2}\rho_O(D_O)^{1.25}(1/(O/F))^{1/2}$, (lb mass/sec)(1/in.$^{3/4}$)	Stability classification
			Hydrogen, T_H	Oxygen, T_O		Hydrogen, ΔP_H	Oxygen, ΔP_O	Hydrogen, W_H	Oxygen, W_O				
C	609	1.9	174	205	311	52.7	193.1	10.82	51.06	4.72	95.6	6.167	Transition
	610		204	183	318	68.1	175.8	10.34	48.27	4.66	103.4	8.066	Stable
	611		172	183	312	56.1	191.3	10.36	44.52	4.30	107.2	6.752	Transition
	614		168	177	315	44.2	180.9	10.30	49.46	4.80	100.7	5.877	Transition
	615		173	204	318	61.1	158.4	12.37	44.36	3.75	101.8	7.339	Stable
	616		165	173	310	43.3	187.4	10.13	49.55	4.89	99.7	5.837	Transition
	618		171	219	319	48.0	203.9	10.16	39.95	3.93	119.2	6.025	
	622		177	262	321	0	0	11.88	46.63	3.93	103.3	-----	
	624		175	202	341	55.0	227.2	11.54	57.18	4.96	95.5	5.974	
	629		171	182	310	43.2	195.2	10.64	49.33	4.64	97.9	5.975	
	634		156	142	314	43.0	192	10.52	52.24	4.97	96.3	5.920	
	661		163	244	326	62.1	234.4	13.01	49.31	3.79	105.3	7.082	
	662		203	238	311	40.7	298.9	9.79	50.86	5.20	98.8	5.357	
	664		190	177	316	48.7	198.9	9.47	51.30	5.49	100.6	6.177	
	665		193	240	317	48.2	272.0	9.26	50.23	5.42	103.4	5.131	
	668		150	194	313	46.7	173.7	10.78	55.39	5.14	90.9	5.191	
	669		145	152	316	56.7	166.5	10.29	52.74	5.12	96.1	6.242	
	670		146	153	316	69.4	159.7	10.35	52.59	5.08	96.0	6.947	
	671		156	163	314	47.2	165.1	10.35	51.57	4.98	96.8	5.892	
	672	↓	110	165	312	56.1	164.9	12.08	48.74	4.04	95.4	5.750	↓

TABLE II. - Continued. EXPERIMENTAL DATA

(b) SI units

Test series	Test	Contraction ratio, $\mathscr{A}$	Hydrogen injection-temperature, T_H, K	Static pressure at injector, P, kN/m^2 abs	Injector pressure drop, kN/m^2		Propellant weight flow, kg/sec		Oxidant-fuel ratio, O/F	Efficiency of characteristic exhaust velocity, η_{C^*}, percent	Stability-limit parameter, $\mathscr{K}_{cr}$, $(2g\Delta P_H/\rho_H)^{1/2}\rho_O(D_O)^{1.25}(1/(O/F))^{1/2}$, $(kg/sec)(1/m^{3/4})$	Stability classification
					Hydrogen, ΔP_H	Oxygen, ΔP_O	Hydrogen, W_H	Oxygen, W_O				
C	38	1.5	67.2	1648	170	889	4.21	20.71	4.92	100.8	31.228	Transition
	39	↓	56.1	1655	224	878	4.98	19.74	3.96	99.2	35.040	↓
	40		81.7	1689	183	1048	3.84	22.48	5.86	101.0	32.588	
	41		57.8	1689	179	851	4.65	20.55	4.42	100.4	29.960	
	42		73.9	1703	193	917	4.12	21.86	5.30	104.1	33.307	Stable
	44		73.3	1689	182	999	4.10	21.99	5.36	100.4	31.911	Transition
A	57	1.9	80.6	1365	134	505	2.86	14.65	5.13	99.1	33.278	Transition
	58		67.8	1372	160	449	3.34	13.60	4.07	99.7	36.447	Transition
	59		91.1	1393	107	486	2.54	15.42	6.07	101.8	29.654	Stable
	60		74.4	1379	146	561	3.17	14.56	4.59	97.1	34.147	Transition
	61		88.3	1386	138	536	2.69	15.24	5.64	99.9	33.144	Transition
	62		82.8	937.5	106	209.5	1.90	9.96	5.24	101.0	36.931	Stable
	63		83.9	931.0	96.5	267	1.89	10.04	5.28	99.8	34.254	Transition
	64		65.0	931.0	97.8	227	2.17	9.21	4.25	101.1	33.471	Transition
	65		95.0	937.5	115	241	1.68	10.66	6.19	103.1	38.141	Stable
	66		85.0	937.5	101	198	2.02	9.61	4.77	101.6	38.326	Stable
	67		62.8	2730	-----	1799	6.07	29.37	4.84	96.7	------	Unstable
	68		61.7	2751	-----	1620	7.10	27.54	3.88	97.6	------	Unstable
	70	↓	62.8	2737	-----	1751	6.44	28.70	4.46	96.9	------	Unstable
B	255	3.0	145	1861	86.0	475	2.65	14.16	5.35	93.2	30.787	Transition
	256		81.1	1992	124	426	3.29	12.85	3.90	100	30.395	↓
	257		135.6	1985	89.6	519	2.62	15.16	5.78	95.4	28.238	
	258		82.8	2137	127.5	506	3.23	14.14	4.39	100.2	28.501	
	259		92.8	2075	131	463	3.04	14.19	4.66	99.0	30.417	
	290		129.5	1868	98	491	2.41	14.75	6.13	-----	28.800	
	291		72.2	1896	145	389	3.62	13.31	3.67	-----	32.296	↓
	292		68.9	2206	241	424	3.79	13.24	3.49	101.5	38.569	Stable
	293		91.1	2116	138	495	3.02	14.29	4.74	98.2	30.075	Transition
	294	↓	110.6	2178	118	607	2.95	15.63	5.29	95.8	28.949	Transition

TABLE II. - Continued. EXPERIMENTAL DATA

(b) Continued. SI units

Test series	Test	Contraction ratio, $\mathscr{A}$	Hydrogen injection-temperature, T_H, K	Static pressure at injector, P, kN/m^2 abs	Injector pressure drop, kN/m^2		Propellant weight flow, kg/sec		Oxidant-fuel ratio, O/F	Efficiency of characteristic exhaust velocity, η_{C^*}, percent	Stability-limit parameter, $\mathscr{W}_{cr}$, $(2g\Delta P_H/\rho_H)^{1/2}\rho_O(D_O)^{1.25}(1/(O/F))^{1/2}$, $(kg/sec)(1/m^{3/4})$	Stability classification
					Hydrogen, ΔP_H	Oxygen, ΔP_O	Hydrogen, W_H	Oxygen, W_O				
B	274	4.5	195.0	2178	101.3	292	1.82	10.92	6.00	96.9	33.036	Stable
	275	↓	150.0	2185	76	326	1.98	11.42	5.76	91.7	26.322	Transition
	277		127.8	2172	89.6	308	2.17	10.60	4.89	93.2	28.736	↓
	279		96.7	2172	103	275	2.39	9.65	4.03	96.9	29.348	
	280		106.1	2178	95	289	2.36	10.37	4.40	92.2	28.352	
	281		196.7	2178	121	409	1.96	12.73	6.49	----	35.942	
	282	↓	134.4	2178	130	396	2.400	12.38	5.16	----	34.446	↓
	326	1.5	63.9	2385	276	1699	6.25	29.98	4.80	98.7	31.497	Transition
	327	↓	70.0	2440	276	1936	5.64	31.70	5.62	100.6	30.758	↓
	328		60.6	2254	321	696	6.22	27.32	4.39	99.7	35.000	
	329		67.8	2419	245	1916	5.83	31.22	5.35	99.6	29.149	
	330	↓	67.2	2389	314	2047	5.85	32.01	5.47	97.1	31.990	↓
A, B, and C	331	1.9	62.2	2289	272	962	5.75	21.91	3.81	100.3	35.251	Transition
	333	↓	75.0	2468	272	1251	5.01	25.59	5.11	100.9	33.471	Transition
	335		91.1	2337	396	1209	4.35	25.30	5.81	101.0	43.545	Stable
	336		66.7	2268	231	995	5.07	22.78	4.51	100.1	31.705	Transition
	337	↓	75.6	2344	224	1119	4.72	24.45	5.18	100.8	31.413	Transition
C	493	3.0	75.0	3454	163.0	1056	5.82	21.28	3.66	101.8	26.351	Transition
	494	↓	135.0	3254	175	1277	4.16	23.71	5.69	98.4	32.687	↓
	495		86.7	3419	138.5	1084	5.17	22.90	4.43	97.8	25.924	
	496	↓	140.6	3247	198	1233	4.30	23.51	5.46	97.7	36.219	↓

TABLE II. - Concluded. EXPERIMENTAL DATA

(b) Concluded. SI units

Test series	Test	Contraction ratio, ε	Injection temperature, K		Static pressure at injector, P, kN/m^2	Injector pressure drop, kN/m^2		Propellant weight flow, kg/sec		Oxidant-fuel ratio, O/F	Efficiency of characteristic exhaust velocity, η_{C^*}, percent	Stability-limit parameter, $\mathscr{W}_{cr}$, $(2g\,\Delta P_H/\rho_H)^{1/2}\rho_O(D_O)^{1.25}(1/(O/F))^{1/2}$, $(kg/sec)(1/m^{3/4})$	Stability classification
			Hydrogen, T_H	Oxygen, T_O		Hydrogen, ΔP_H	Oxygen, ΔP_O	Hydrogen, W_H	Oxygen, W_O				
C	609	1.9	96.7	113.9	2144	363	1331	4.90	23.13	4.72	95.6	43.909	Transition
	610		113.3	101.7	2192	469	1212	4.68	21.87	4.66	103.4	57.429	Stable
	611		95.6	101.7	2151	387	1319	4.69	20.17	4.30	107.2	48.074	Transition
	614		93.3	98.3	2172	305	1247	4.66	22.41	4.80	100.7	41.844	Transition
	615		96.1	113.3	2192	421	1092	5.60	20.09	3.75	101.8	52.253	Stable
	616		91.7	96.1	2137	298	1292	4.59	22.45	4.89	99.7	41.559	Transition
	618		95.0	121.6	2199	331	1406	4.60	18.09	3.93	119.2	42.898	
	622		98.3	145.5	2213	---	----	5.38	21.12	3.93	103.3	------	
	624		97.2	112.2	2351	379	1566	5.23	25.90	4.96	95.5	42.535	
	629		95.0	101.1	2137	298	1346	4.82	22.35	4.64	97.9	42.542	
	634		86.7	78.9	2165	296	1324	4.76	23.66	4.97	96.3	42.150	
	661		90.6	135.6	2247	428	1616	5.89	22.34	3.79	105.3	50.424	
	662		112.8	132.2	2144	281	2061	4.43	23.04	5.20	98.8	38.141	
	664		105.6	98.3	2178	336	1371	4.29	23.24	5.49	100.6	43.980	
	665		107.2	133.3	2185	332	1875	4.19	22.75	5.42	103.4	36.536	
	668		83.3	107.8	2158	322	1197	4.88	25.09	5.14	90.9	36.959	
	669		80.6	84.4	2178	391	1148	4.66	23.89	5.12	96.1	44.443	
	670		81.1	85.0	2178	478	1101	4.69	23.82	5.08	96.0	49.463	
	671		86.7	90.6	2165	325	1138	4.69	23.36	4.98	96.8	41.951	
	672		61.1	91.7	2151	387	1137	5.47	22.08	4.04	95.4	40.940	

transition (minimum stable hydrogen temperature) is shown as a function of the oxidant-fuel ratio for four different chamber pressures and weight-flow-per-element operating conditions. The region above the curve represents a region of stable operation and, conversely, unstable operation below the curve. Typical of the hydrogen-temperature stability limits of reference 1, the screech limit defined by the data was approximately a linear function of the oxidant-fuel ratio. The hydrogen-temperature stable operating range improved as the oxidant-fuel ratio was decreased. More important, however, is the fact that the simultaneous variations in the propellant weight flow and chamber pressure had no effect on the stability of the combustor, as measured by hydrogen temperature. At an oxidant-fuel ratio of 5, the screech transition temperature was 140° R (78 K) for the range of chamber pressure (125 to 380 psia or 862 to 2620 kN/m^2 abs) investigated.

Effect of contraction ratio and weight flow per element at constant chamber pressure. - Experiments to determine the effect of changes in the nozzle contraction ratio on stability (test series B) were conducted at a nominal chamber pressure of 300 psia (2070 kN/m^2 abs). The propellant weight flow per element was varied, as required by the change made in nozzle throat area to maintain the chamber pressure at 300 psia (2070 kN/m^2 abs). The program included four variations in the nozzle throat diameter, 8.78, 7.82, 6.22, and 5.04 inches (22.3, 19.85, 15.8, and 12.8 cm) which corresponded to contraction ratios of 1.5, 1.9, 3.0, and 4.5, respectively. As done previously, the stability of the combustor was rated in terms of the minimum stable hydrogen-injection temperature. Examination of the results of figure 7 shows that screech occurred at widely different values of hydrogen temperature as the propellant weight flow and contraction ratio were varied. For example, the transition temperature for the combustor with a contraction ratio of 4.5 was 240° R (133 K) (O/F of 5) as compared with 118° R (66 K) for the combustor with a contraction ratio of 1.5.

Effect of contraction ratio and chamber pressure at constant weight flow per element. - Experiments in the third phase of the investigation (test series C) were similar to those in test series B except that the total propellant flow was held constant. Therefore, the chamber pressure varied in proportion to the change in the contraction ratio. The same combustor configurations as those of test series B were used. Curves of the hydrogen temperature limit as a function of the oxidant-fuel ratio are presented for the various contraction-ratio combustors (contraction ratios of 1.5, 1.9, and 3) in figure 8. The combustor with a contraction ratio of 4.5 was not evaluated because of pressure limitations of the facility propellant tank. Similar to the effects of contraction ratio, established in test series B (fig. 7), the results show a loss in stability (minimum stable hydrogen temperature) as the nozzle contraction ratio was increased (nozzle throat diameter decreased). In fact, if the results are compared, the stability-limit curves are about the same for both series.

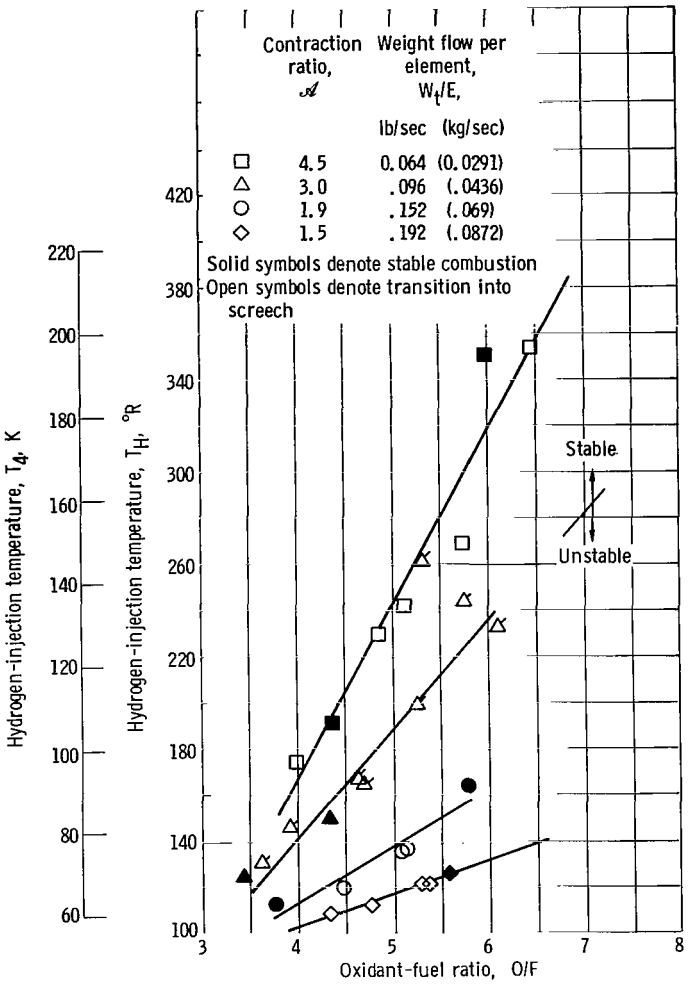

Figure 7. - Effect of nozzle contraction ratio on variation of screech transition temperature. Chamber pressure, 300 psia (2070 kN/m^2 abs).

Effect of oxygen-injection temperature. - Although the effect of the oxygen temperature (density) is not directly related to the test matrix used to delineate the effects of chamber pressure, thrust per element, and contraction ratio, it is included herein as a matter of interest. Presented in figure 9 are results of a brief series of tests wherein the hydrogen-temperature stable operating limits were determined at oxygen-injection temperatures that varied from 140° to 240° R (78 to 133 K) and corresponded to densities of 0.0435 and 0.0315 pound per cubic inch (1200 to 871 kg/cu m), respectively. The injector used was the same design as the one used to investigate the effects of chamber pressure, thrust per element, and contraction ratio; however, the baseline stability limits of the injector had shifted, possibly because of deterioration. Nevertheless,

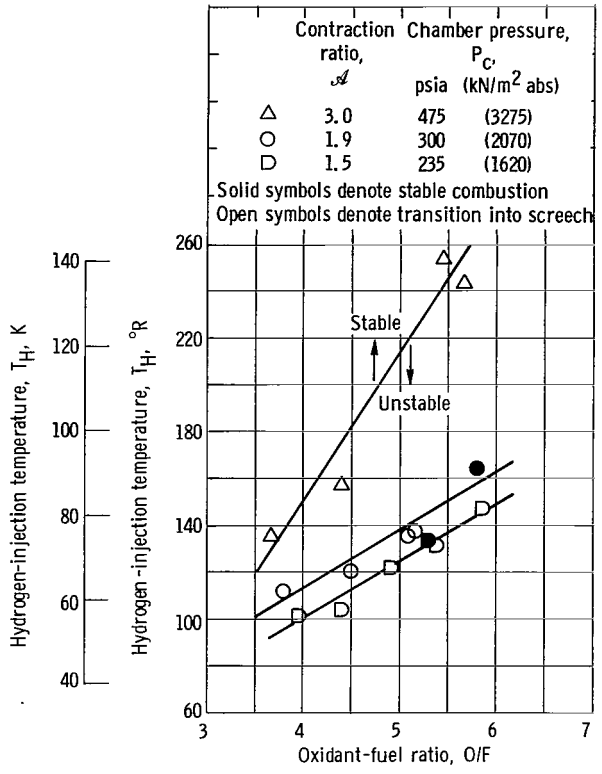

Figure 8. - Effect of chamber pressure and contraction ratio on variation of screech transition temperature. Weight flow per element, 0.152 pound per second (0.069 kg/sec).

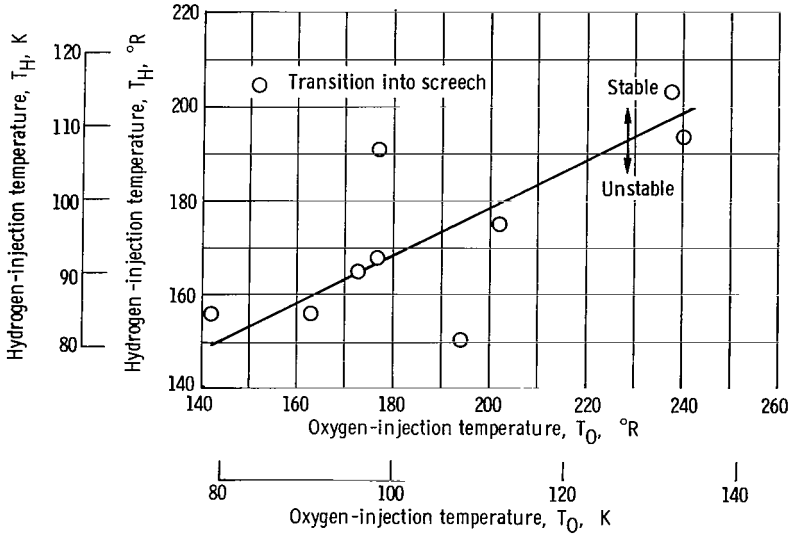

Figure 9. - Variation of hydrogen-temperature stable operating limits with oxygen-injection temperature. Oxidant-fuel ratio, 4.75 to 5.5.

examination of figure 9, wherein hydrogen stable operating limits are plotted, shows that increasing the oxygen-injection temperature has a strong destabilizing effect on the combustion process. The hydrogen transition temperature increased by about 50° R (27.8 K) over the range of oxygen temperatures investigated.

Screech Characteristics

Typical plots of pressure amplitude against frequency, obtained from a spectrum analysis of chamber pressure during screech, are presented in figures 10 to 12 for each test series (table I). With the exception of the tests conducted at low chamber pressure, the predominant mode of instability, which was triggered spontaneously by the ramped hydrogen-injection temperature, was the first tangential acoustic mode. The calculated frequency corresponding to this mode for the chamber diameter and environment varies between 3000 and 3500 cps (3000 and 3500 Hz), depending on the oxidant-fuel ratio. In most tests, lesser pressure amplitudes at frequencies of about 3800 (second longitudinal), 6800, and 7200 cps (3800, 6800, and 7200 Hz) were also present. At chamber-pressure operating conditions (nominal) of 200 and 135 psia (1376 and 961 kN/m^2 abs), the first tangential acoustic mode was again triggered spontaneously, but later in the run (figs. 10(c) and (d)), the predominant mode of instability changed to the second tangential acoustic mode (5500 to 6000 cps or 5500 to 6000 Hz). The amplitude of the pressure oscillation, however, remained about the same for all chamber-pressure operating conditions investigated. Contraction-ratio variations at a constant chamber pressure (fig. 11) or at a constant weight flow per element (fig. 12) had no apparent effect on screech amplitude or mode.

Combustion Performance

The combustion performance of the injector at the minimum stable hydrogen-injection temperature for each test conducted in the program is shown in figure 13. Characteristic exhaust-velocity efficiency, based on equilibrium composition, is presented as a function of the oxidant-fuel ratio. It should be noted that the performance data were obtained under transient conditions; thus, a considerable amount of scatter due to time-constant variations between instruments is present in the results, which occasionally yields results greater than 100 percent. Varying the total propellant flow to affect a change in chamber pressure (test series A) had no significant effect on combustion performance (fig. 13(a)). The characteristic exhaust-velocity efficiency remained nearly constant at about 100 percent over the entire range of chamber pressure (weight flow per element) investigated.

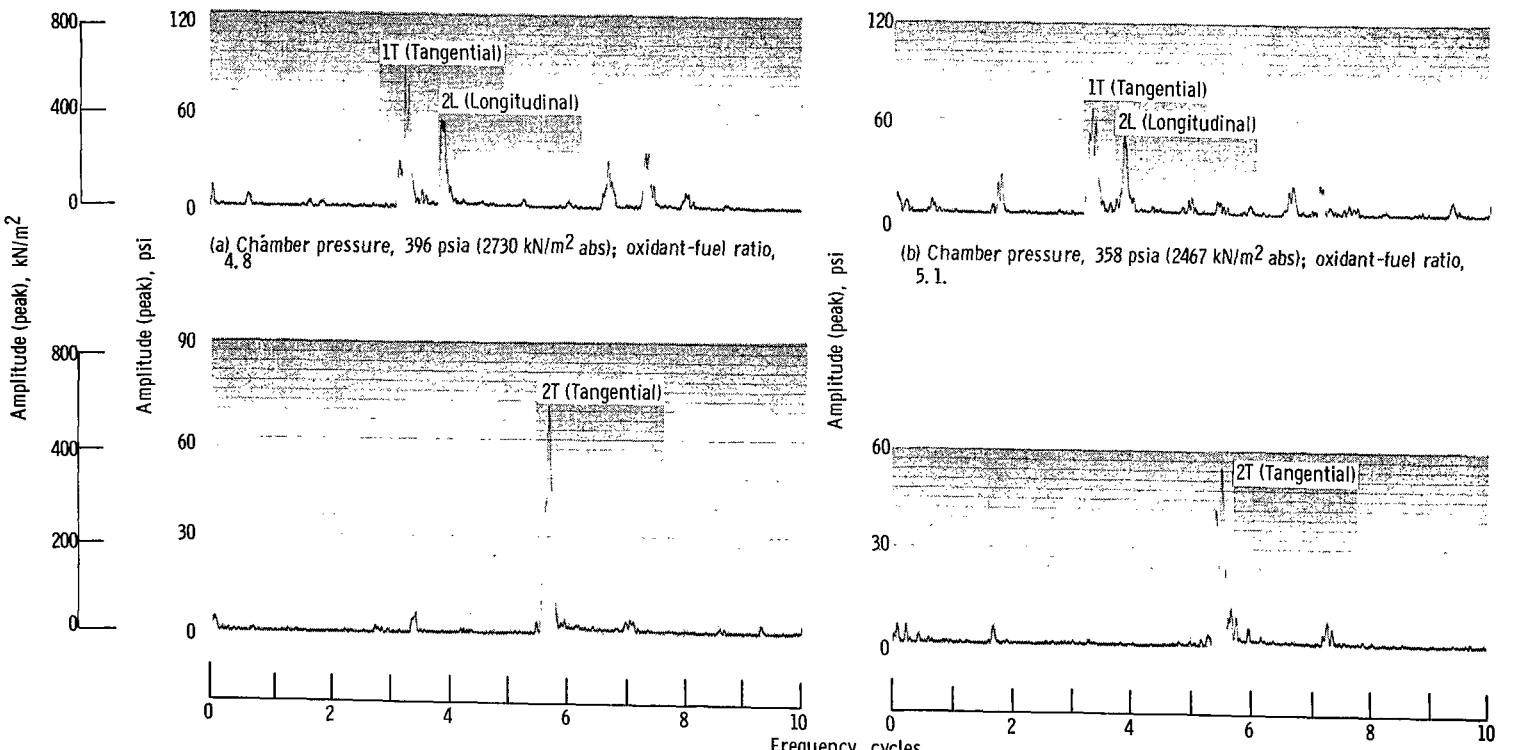

Figure 10. - Typical pressure-amplitude spectral density traces for test series A. Contraction ratio, 1.9.

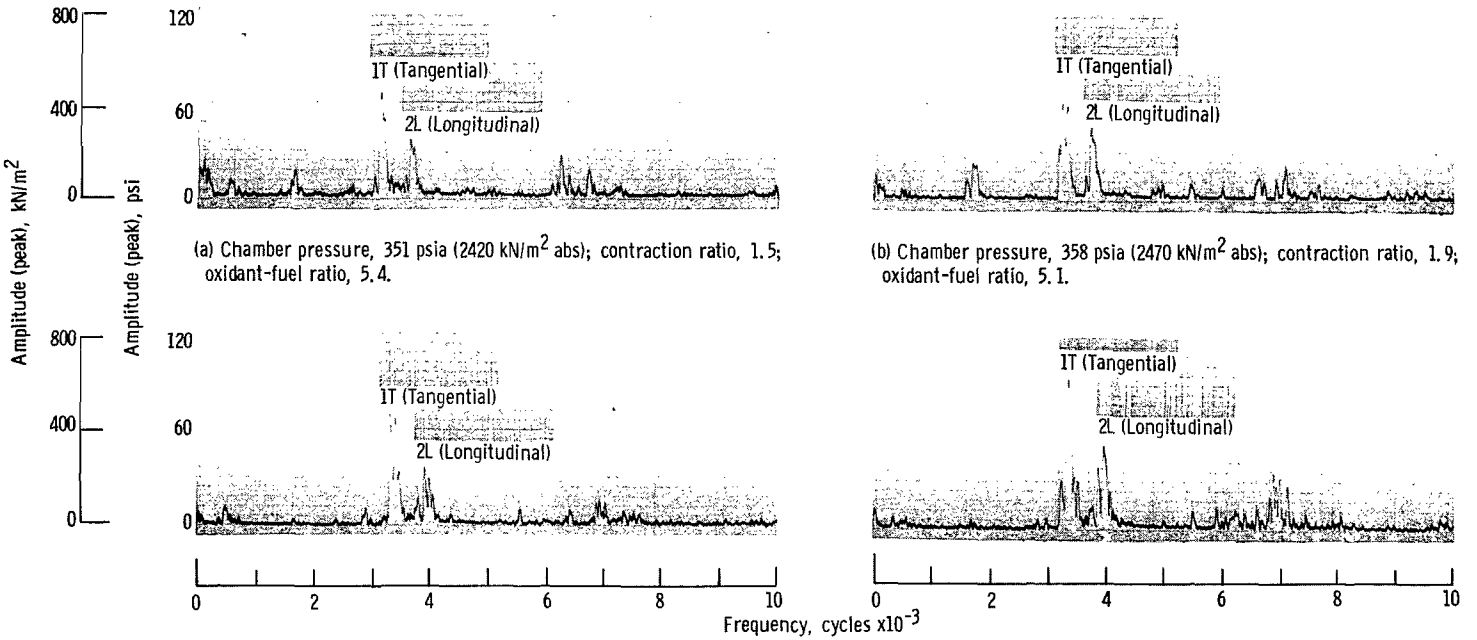

(a) Chamber pressure, 351 psia (2420 kN/m^2 abs); contraction ratio, 1.5; oxidant-fuel ratio, 5.4.

(b) Chamber pressure, 358 psia (2470 kN/m^2 abs); contraction ratio, 1.9; oxidant-fuel ratio, 5.1.

(c) Chamber pressure, 278 psia (1916 kN/m^2 abs); contraction ratio, 3; oxidant-fuel ratio, 5.2.

(d) Chamber pressure, 317 psia (2185 kN/m^2 abs); contraction ratio, 4.5; oxidant-fuel ratio, 4.9.

Figure 11. - Typical pressure-amplitude spectral density traces for test series B.

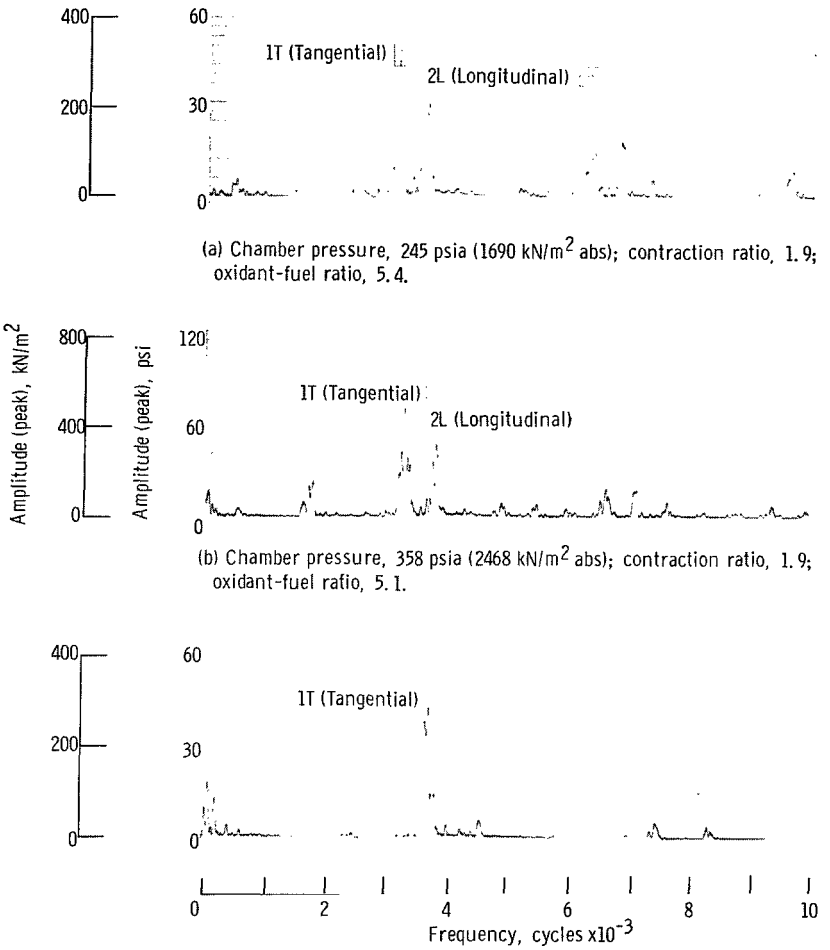

(a) Chamber pressure, 245 psia (1690 kN/m^2 abs); contraction ratio, 1.9; oxidant-fuel ratio, 5.4.

(b) Chamber pressure, 358 psia (2468 kN/m^2 abs); contraction ratio, 1.9; oxidant-fuel ratio, 5.1.

(c) Chamber pressure, 501 psia (3453 kN/m^2 abs); contraction ratio, 3; oxidant-fuel ratio, 3.5.

Figure 12. - Typical pressure-amplitude spectral density traces for test series C.

In figure 13(b) are presented performance results of test series B, during which the contraction ratio was varied from 1.5 to 4.5, and, simultaneously, the total propellant flow was changed as required to maintain chamber pressure. Examination of the results shows that the combined effect of decreasing the total weight flow per element and the free-stream Mach number (increasing contraction ratio) was detrimental to performance. The characteristic exhaust-velocity efficiency of the combustor with a nozzle contraction ratio of 4.5 was about 94 percent, which represents a decrease of about 5 percentage points as compared with the performance of the combustors with contraction ratios of 1.5 or 1.9. The loss in performance may possibly result from a change in the oxygen droplet vaporization length. The larger drop size associated with low injection velocities and the lower droplet combustion-gas-velocity differential have adverse effects on the vaporization

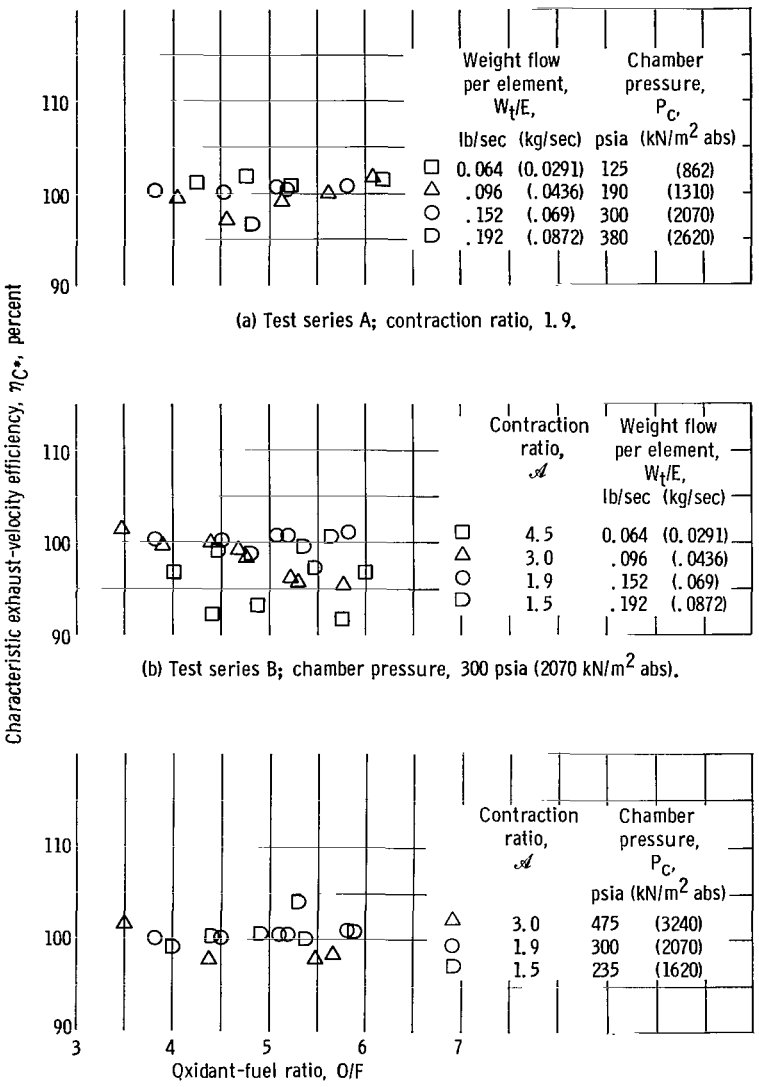

(a) Test series A; contraction ratio, 1.9.

(b) Test series B; chamber pressure, 300 psia (2070 kN/m^2 abs).

(c) Test series C; total weight flow per element, 0.152 pounds per second (0.069 kg/sec).

Figure 13. - Combustion performance of 421-element concentric-tube injector at screech transition temperature.

length. In test series C, which also included a variation in the nozzle contraction ratio, any significant effect of contraction ratio on performance in these data was difficult to ascertain (fig. 13(c)). A decrease in performance of about 1 to 2 percent was observed in three tests out of four with the contraction ratio of 3; however, this variation is about equal to the estimated accuracy of the data.

Correlation of Stability Data

The present data and those of reference 1 constitute a considerable amount of data over a wide range of geometric variables and operating conditions from which it should be possible to determine the critical parameters affecting the stability of hydrogen-oxygen engines. A correlation was obtained which considered all the experimental data. The form of the parameter was guided by interpretation of the data according to the response-factor model of reference 2. The correlating parameter $\mathscr{W}_{cr}$ represents the stability limit over the range of variables investigated and is given by

$$\left(\frac{2g\ \Delta P_H}{\rho_H}\right)^{1/2} \rho_O (D_O)^{1.25} \left(\frac{1}{O/F}\right)^{1/2}$$

where

ΔP_H hydrogen-injector pressure drop

ρ_H hydrogen-injection density

ρ_O oxygen-injection density

D_O oxygen-injection orifice diameter

O/F oxidant-fuel ratio

Transition data for all the experiments in the present study are plotted against oxidant-fuel ratio in the form of this parameter in figure 14, and the data of reference 1 are plotted in figure 15. The average value of the parameter, excluding the data for varying oxygen temperature, was 4.4. In these figures, the area above the line represents a region of stable operation and, conversely, unstable operation below the line. The standard deviation of the present data was 9 percent and 17.5 percent for the data of reference 1. Note that the recessed-oxygen-tube data are included in the correlation presented in figure 15. Although these recessed-element data in general have values of the

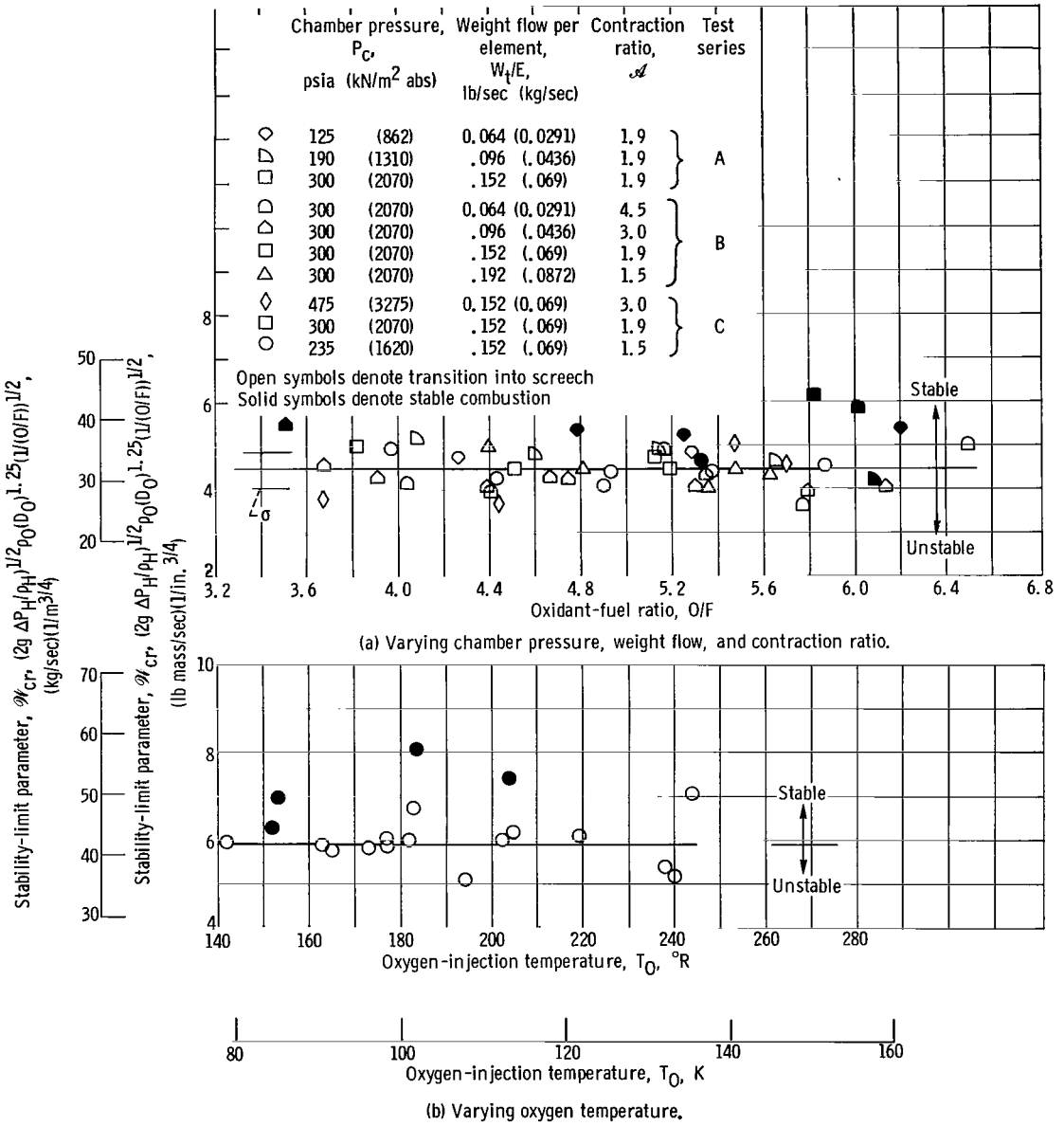

(a) Varying chamber pressure, weight flow, and contraction ratio.

(b) Varying oxygen temperature.

Figure 14. - Correlation of stability limits of 421-element injector at various operating conditions.

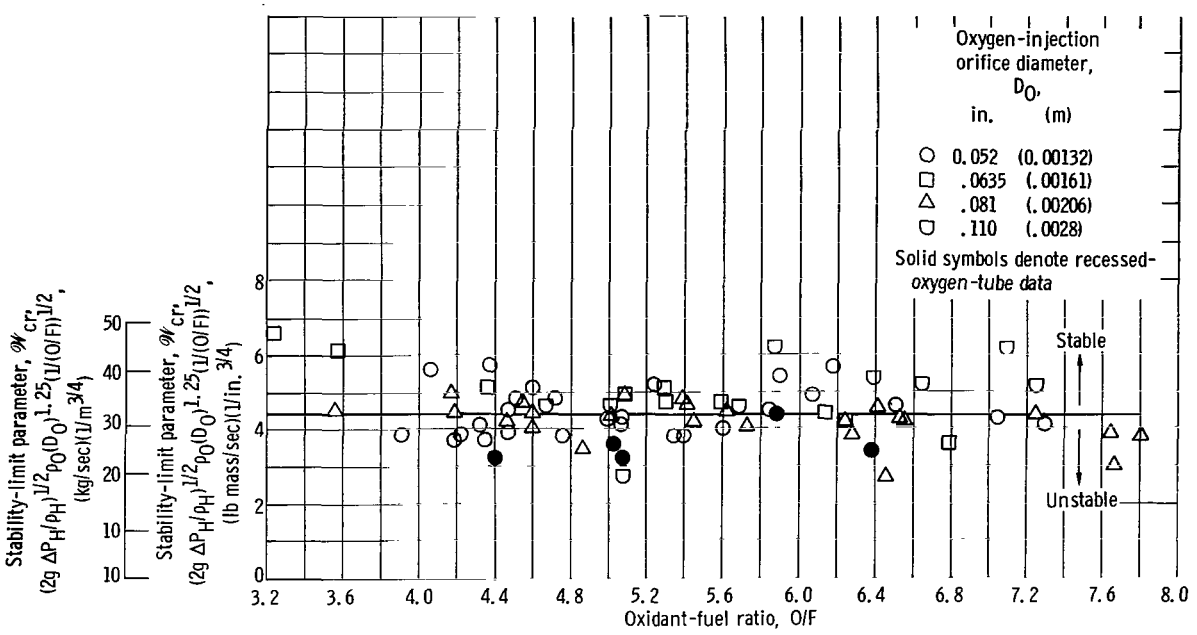

Figure 15. - Correlation of stability limits of various 421-element concentric-tube injector configurations. (Data from ref. 1.)

constant slightly less than the average value for the data, they had never been correlated previously. The experiments in which oxygen density was varied show a higher value of 5.9 for the constant (fig. 14(b)). As discussed earlier, this value was attributed to the possible deterioration of the injector, and for this reason the data are not included in the determination of the constant or the standard deviation.

This representation of the stability limit is considerably different from the previous correlation presented in reference 1 wherein the limit was represented by a constant value of the injection velocity ratio. The modification whereby the hydrogen velocity was replaced by $(2g\ \Delta P_H/\rho_H)^{1/2}$ was suggested by the response-factor model and was supported by the fact that the modified form provided a better correlation of the recessed-element data. The present study indicates that stability is influenced by the oxygen density and jet diameter rather than by oxygen injection velocity. The oxygen-jet-diameter dependency was obtained by fitting the data of reference 1. Likewise, the oxidant-fuel-ratio dependency was obtained by the best fit of the data. Undoubtedly, other forms of the parameter exist that would similarly correlate the data; however, the form presented shows the combined effect of all geometric and operating variables investigated thus far.

Application of Response-Factor Model to Experiment

The response-factor model presented in reference 2 assumes that the stability of an

engine is controlled by the dynamic coupling that occurs between chamber-pressure oscillations and the various combustion or flow processes. If the total coupling produces a large enough in-phase addition, instability will result. For gaseous-hydrogen - liquid-oxygen engines, this coupling has been evaluated in the form of a response factor, a measure of in-phase addition, for three processes. These processes are the response of the hydrogen flow (ref. 2), the response of vaporizing liquid-oxygen drops (ref. 5), and the response of the nozzle flow (ref. 2). In reference 2, analytical results from the model were compared with some of the experimental results from reference 1. For the particular experiments studied, the hydrogen-injection area and oxidant-fuel ratio were the primary variables, and the model predicted quite well the experimentally observed variation of the stability limit with the hydrogen-injection area and oxidant-fuel ratio. Reference 2 concluded that the mechanism assumed for the hydrogen system in the model, coupling between the hydrogen flow and chamber-pressure oscillations, could be an important factor in instability in gaseous-hydrogen - liquid-oxygen engines. In the present study, chamber pressure and propellant flow rate were the primary variables. The influence of these parameters on the experimental stability limits can be explained by their influence on the hydrogen response factor in the model while the remaining two response factors are kept constant. Details of the model and its application are given in references 2 and 6.

The hydrogen response factor is plotted against hydrogen-injection density in figure 16 for several flow-rate - chamber-pressure combinations. These curves are for a mixture ratio of 5.5 and an oscillation frequency of 3400 cps (3400 Hz). In reference 2, one set of data was fitted to determine the time delay τ_b, which was 0.00009 second. For

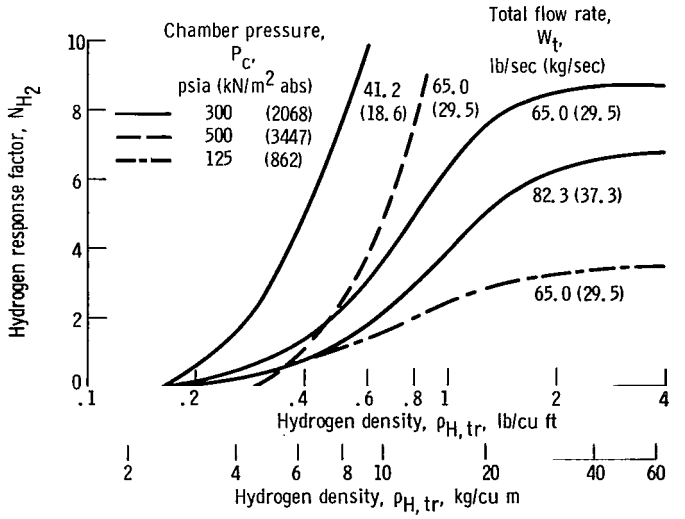

Figure 16. - Effect of flow rate and chamber pressure on response-factor - density characteristics. Oxidant-fuel ratio, 5.5.

the present data, τ_b was changed to 0.00008 second to obtain a slightly better fit. It can be seen (fig. 16) that, as the hydrogen density is increased (temperature is decreased), the response factor increases. The rate of increase is more rapid for lower flow rates. A similar effect occurs for the higher chamber pressures.

The value of the hydrogen-response factor N_{H_2} needed to satisfy the stability criterion (ref. 2) is 2.39 at a mixture ratio of 5.5. From figure 16, the density corresponding to this value can be obtained for given conditions. Figures 17 to 19 show the variation of hydrogen transition density thus obtained against flow rate (varying nozzle area) at constant chamber pressure, flow rate (varying chamber pressure) at constant throat area, and chamber pressure (varying nozzle area and flow rate), respectively. Also shown in figures 17 to 19 are the experimental transition densities that were obtained under conditions nominally equivalent to those used for calculating the analytical curves. The predominant effect for the three variables was associated with flow rate. Thus, in figure 19 several flow rates corresponding to the experimental data were needed to relate the analysis and experiment. In the range of chamber pressure investigated in test series C, hydrogen transition density is almost independent of chamber pressure. Below a chamber pressure of 225 psia (1550 kN/m^2 abs), however, the model predicts that the transition density will increase or that the stable operating limits will increase as the chamber pressure is decreased.

The agreement between experiment and theory, as shown by these figures, was good. Of interest is that the oxygen response was treated as invariant over the range of parameters experimentally studied to obtain this correlation. In general, it might have been

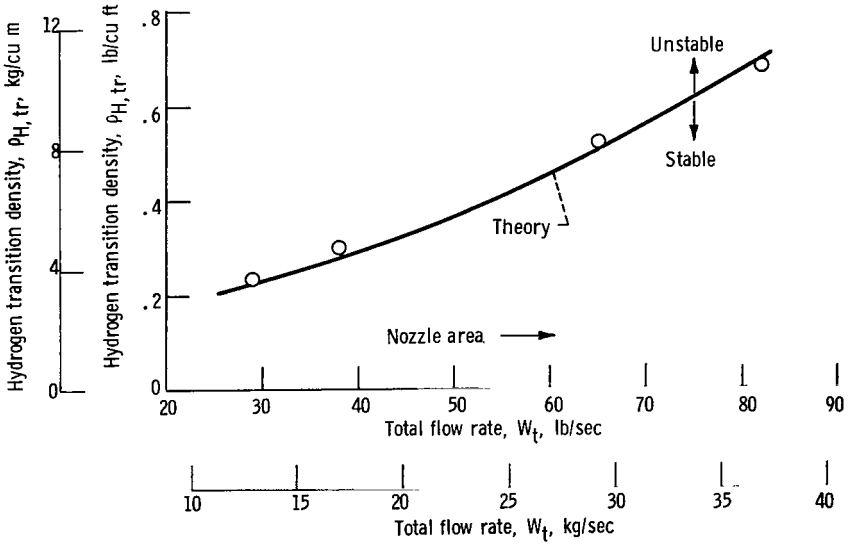

Figure 17. - Effect of flow rate on hydrogen transition density at constant chamber pressure. Oxidant-fuel ratio, 5.5; chamber pressure, 300 psia (2068 kN/m^2 abs).

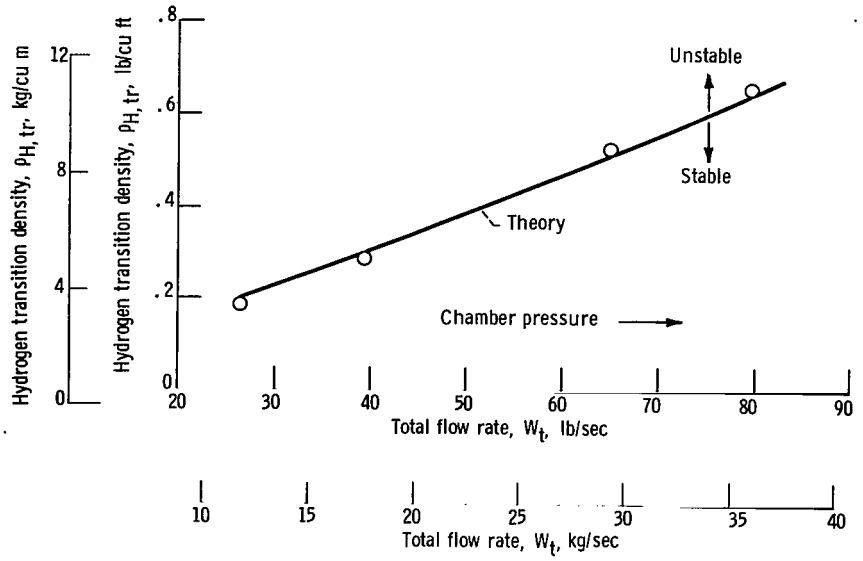

Figure 18. - Effect of flow rate on hydrogen transition density at constant contraction ratio of 1.9. Oxidant fuel-ratio, 5.5.

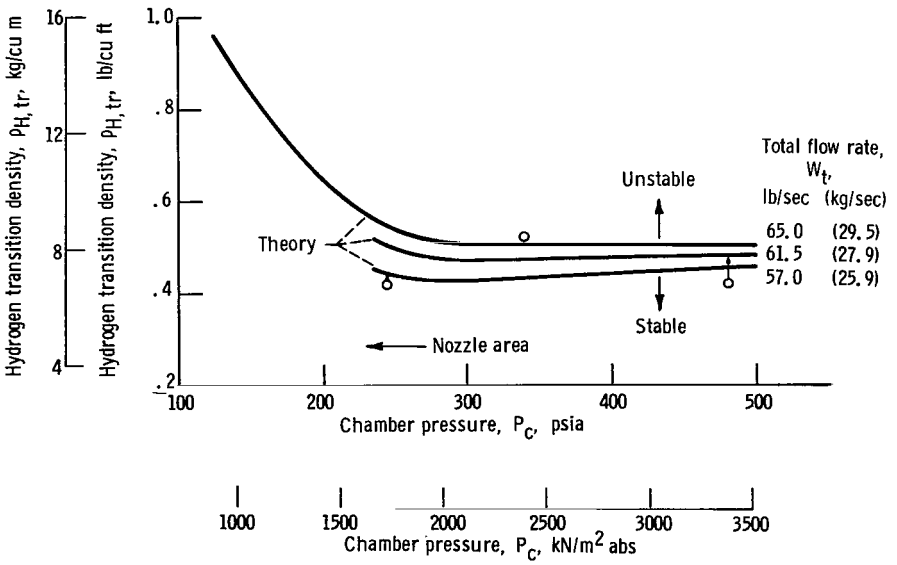

Figure 19. - Effect of chamber pressure on hydrogen transition density. Oxidant-fuel ratio, 5.5.

expected that over this range a variation of the oxygen response factor would have been necessary; however, it was not. The behavior observed is thus associated with the hydrogen response factor and, more particularly, with the resistance terms in the response factor represented by the hydrogen-injection pressure drop. Therefore, when the pressure drop becomes small enough, the hydrogen flow couples with and drives the chamber-pressure oscillations. Since figures 17 and 18 show an almost linear variation of the hydrogen transition density with flow rate and since the hydrogen-injection area was constant, the transition boundary is approximately represented by a constant hydrogen-injection velocity, even though the oxygen velocity varied over a three-to-one range. This result is in agreement with the empirical correlation, which also shows that the oxygen enters into the stability limit only when the oxygen temperature (density) or the orifice diameter are varied. The drop size produced by the injector can be expected to vary with the injector orifice diameter. Also, since the oxygen response factor depends strongly on the drop size (ref. 5), a large change might be expected to occur in the stability limit with an orifice diameter change. The effect of oxygen temperature is less obvious; however, it may be associated with the physical properties of the liquid.

Application and Interpretation of Results

A functional representation of the pressure-density-temperature behavior of low-temperature hydrogen gas was used to obtain a stability equation in terms of the hydrogen temperature. From the data of reference 7, the interdependence of pressure, density, and temperature is approximately given by

$$P \approx \rho(T_H)^2 \qquad \text{where } 65^\circ\,R \leq T_H \leq 130^\circ\,R \ (36\,K \leq T_H \leq 72\,K)$$

In this temperature region, the correlation parameter provides the following equation for stability determination:

$$T_H\left(\frac{2g\,\Delta P_H}{P_c}\right)^{1/2} \rho_O(D_O)^{1.25}\left(\frac{1}{O/F}\right)^{1/2} \begin{cases} > \mathscr{W}_{cr} \text{(stable combustion)} \\ = \mathscr{W}_{cr} \text{ (transition)} \\ < \mathscr{W}_{cr} \text{ (unstable combustion)} \end{cases} \qquad (1)$$

From these equations, it can be seen that the stability limit $\mathscr{W}_{cr}$ is reached during a temperature ramp by the combined effect of reducing the hydrogen temperature and the hydrogen-injector pressure drop. The reduction in injector pressure drop occurs because of the increase in hydrogen density as the temperature is reduced.

Equation (1) can be rearranged to show the effects of the various parameters on hydrogen transition temperature as

$$T_{H,tr} \approx \left(\frac{P_c}{2g\ \Delta P_H}\right)^{1/2} \frac{1}{\rho_O (D_O)^{1.25}} (O/F)^{1/2} \qquad (2)$$

Although it is an approximation, equation (2) is the form of the stability parameter that provides the most insight into the physical interpretation of instability in hydrogen-oxygen engines. If the parameters of equation (2) related only to the hydrogen system are considered and if the minor contribution of the oxidant-fuel-ratio term is neglected, the hydrogen-injector pressure drop is the real determinant of the screech boundary at any given chamber-pressure operating condition. The hydrogen transition temperature is inversely proportional to the square root of the pressure drop; thus, an increase in pressure drop will lower the hydrogen transition temperature and increase the stable operating range. Note that increasing the pressure drop to promote stability is not limited to making changes in the injection flow area; the same effect on stability may be achieved through changes made in the orifice hydraulic flow characteristics. Parameters that influence stability and are related to the oxygen system are the oxygen density and the oxygen jet diameter. Increasing these parameters will also improve the stable operating range by decreasing the transition temperature.

From equation (2), the effect on stability of the three parameters (chamber pressure, weight flow, and contraction ratio) investigated in the present study can also be shown. In test series A, the three weight-flow - chamber-pressure conditions resulted in the same transition temperature. The chamber pressure and injector pressure drop varied together so that the ratio remained constant and, therefore, no change was produced in the hydrogen transition temperature. The contraction ratio does not appear independently in equation (2); however, the variation in the stability limits with this parameter results from its effect on the total propellant flow and, thus, on the chamber pressure or injector pressure drop. Also, since both chamber pressure and injector pressure drop are nearly proportional to propellant flow, equation (2) shows that the change in the transition temperature with changes in the contraction ratio will be the same regardless of which parameter is allowed to vary, as was determined in test series B and C.

The results of the present study clearly show that a designer can scale thrust upwards by increasing the throat diameter and flow rate, not only without a loss, but with an improvement in the hydrogen-temperature stability margin. In fact, increasing the nozzle throat diameter and simultaneously decreasing the chamber pressure to maintain thrust constant is a technique to improve the stability of an engine.

The hydrogen-temperature stability parameter appears to be a useful design tool, inasmuch as it permits the predictions of a change in screech limits for any change in engine design within the limits of the range of variables covered by the data. This parameter can be used to determine the effect on stability of variations in hydrogen-injection area, oxygen-injection area, oxidant-fuel ratio, oxygen temperature or density, chamber pressure, oxygen element recess, contraction ratio, weight flow per element, and number of injection elements. It must be noted, however, that the parameter has been evaluated only in a single-diameter chamber and at chamber pressures below the critical pressure of oxygen.

SUMMARY OF RESULTS

The high-frequency stability limits were determined over a range of contraction ratios, chamber pressures, and weight flows for a 20 000-pound- (89-kN-) thrust gaseous-hydrogen - liquid-oxygen rocket engine with a single coaxial-type injector. The limits were determined by the technique of ramping hydrogen-injection temperature. The results are as follows:

1. Throttling the total weight flow to change the chamber pressure had no effect on the hydrogen-temperature stable operating limits of the combustor.

2. Decreasing the contraction ratio at either constant weight flow per element or at constant chamber pressure lowered the hydrogen transition temperature.

3. Increasing the oxygen-injection temperature or decreasing the oxygen density increased the hydrogen transition temperature.

4. The stability limit was represented by a constant value of the parameter $(2g\ \Delta P_H/\rho_H)^{1/2}\ \rho_O(D_O)^{1.25}\left[1/(O/F)\right]^{1/2}$, where ΔP_H is the hydrogen-injector pressure drop, ρ_H is the hydrogen-injection density, ρ_O is the oxygen-injection density, D_O is the oxygen-injection orifice diameter, and O/F is the oxidant-fuel ratio. At values of the parameter above 4.4, combustion was stable and was unstable at values below 4.4.

5. The effect of hydrogen-injection area, oxidizer tube recess, and other variations in the injector-element geometry was to influence the resistance to flow. Such effects were accounted for by the term $(\Delta P_H/\rho_H)^{1/2}$.

6. The stability-limit parameter found appeared to account for the experimental trends observed; however, the proportionality constant may change as other injector or chamber parameters are varied.

7. The effect of the oxygen system on stability appeared to be related to the oxygen density and oxygen jet diameter. Increasing either parameter lowered the hydrogen transition temperature and improved the stable operating range.

8. Good agreement was obtained between experimental stability limits and those predicted by the response-factor model. For the present data, the effects that occurred were represented by changes in the hydrogen-coupling mechanism.

Lewis Research Center,
National Aeronautics and Space Administration,
Cleveland, Ohio, April 26, 1968,
128-31-06-05-22.

REFERENCES

1. Wanhainen, John P.; Parish, Harold C.; and Conrad, E. William: Effect of Propellant Injection Velocity on Screech in 20,000-Pound Hydrogen-Oxygen Rocket Engine. NASA TN D-3373, 1966.

2. Feiler, Charles E.; and Heidmann, Marcus F.: Dynamic Response of Gaseous-Hydrogen Flow System and Its Application to High-Frequency Combustion Instability. NASA TN D-4040, 1967.

3. Ladd, J. W.: A Durable and Reliable Test Stand System for High-Accuracy Temperature Measurements in the Cryogenic Ranges of Liquid Hydrogen and Liquid Oxygen. Advances in Cryogenic Engineering. Vol. 6. K. D. Timmerhaus, ed., Plenum Press, 1961, pp. 388-395.

4. Herr, Austin C.; Terbeek, Howard G.; and Tieferman, Marvin W.: Suitability of Carbon Resistors for Field Measurements of Temperature, in the Range 35° to 100° R. NASA TN D-264, 1960.

5. Heidmann, Marcus F.; and Wieber, Paul R.: Analysis of Frequency Response Characteristics of Propellant Vaporization. NASA TN D-3749, 1966.

6. Feiler, C. E.: Effect of Combustor Parameters on the Stability of Gaseous Hydrogen-Liquid Oxygen Engine. Presented at the 4th Combustion Conference, Menlo Park, Calif., Interagency Chemical Rocket Propulsion Group, Oct. 2-13, 1967.

7. Roder, Hans M.; and Goodwin, Robert D.: Provisional Thermodynamic Functions for Para-Hydrogen. Tech. Note 130, National Bureau of Standards, Dec. 1961.

NASA-Langley, 1968 —— 33 E-4355

"The aeronautical and space activities of the United States shall be conducted so as to contribute . . . to the expansion of human knowledge of phenomena in the atmosphere and space. The Administration shall provide for the widest practicable and appropriate dissemination of information concerning its activities and the results thereof."

—NATIONAL AERONAUTICS AND SPACE ACT OF 1958

NASA SCIENTIFIC AND TECHNICAL PUBLICATIONS

TECHNICAL REPORTS: Scientific and technical information considered important, complete, and a lasting contribution to existing knowledge.

TECHNICAL NOTES: Information less broad in scope but nevertheless of importance as a contribution to existing knowledge.

TECHNICAL MEMORANDUMS: Information receiving limited distribution because of preliminary data, security classification, or other reasons.

CONTRACTOR REPORTS: Scientific and technical information generated under a NASA contract or grant and considered an important contribution to existing knowledge.

TECHNICAL TRANSLATIONS: Information published in a foreign language considered to merit NASA distribution in English.

SPECIAL PUBLICATIONS: Information derived from or of value to NASA activities. Publications include conference proceedings, monographs, data compilations, handbooks, sourcebooks, and special bibliographies.

TECHNOLOGY UTILIZATION PUBLICATIONS: Information on technology used by NASA that may be of particular interest in commercial and other non-aerospace applications. Publications include Tech Briefs, Technology Utilization Reports and Notes, and Technology Surveys.

Details on the availability of these publications may be obtained from:

SCIENTIFIC AND TECHNICAL INFORMATION DIVISION

NATIONAL AERONAUTICS AND SPACE ADMINISTRATION

Washington, D.C. 20546